A Novel Resonant Controller Discretization and Design Procedure Based on Inverse Nyquist Diagrams

Fábio A. L. Alves * **André R. de Castro** * **Thiago C. Tricarico** *
Marcello S. Neves * **Maurício Aredes** *

* *Programa de Engenharia Elétrica, Universidade Federal do Rio de Janeiro, Rio de Janeiro, RJ, (e-mail: fabioleitealves@lemt.ufrj.br, andrerc@lemt.ufrj.br, thiago@lemt.ufrj.br, marcello@lemt.ufrj.br, aredes@lemt.ufrj.br.*

Abstract: Resonant controllers, whether Resonant Proportional (PR) or Vectorial Proportional Integral (VPI), are increasingly used in power electronics converters. Since they are most often embedded in digital microcontrollers, the discretization effects of their mathematical models directly impact the dynamics of the final system. This paper proposes a new discretization for the PR and VPI resonant controllers. Allied to this proposition, a design algorithm focused on optimizing the closed-loop stability of the system via inverse Nyquist diagrams and harmonic current compensation is also proposed. Simulation results prove the validity of the proposed discretization as well as the design algorithm.

Keywords: Resonant Controllers, Discretization Techniques, Inverse Nyquist Diagram, Harmonic Compensators, Current Controlled VSC

1. INTRODUCTION

Resonant controllers are controllers that have recently become popular due to their variety of applications in power electronics converters. They have the ability to track sinusoidal references and good dynamic behavior. In addition, they allow the compensation of harmonic currents to be made simple, due to their characteristic selectivity with respect to the frequencies at which they are tuned. Two most commonly used types of resonant controllers are Proportional Resonant (PR) and Vectorial Proportional Integral (VPI).

The digital implementation of these controllers in microprocessors is of utmost importance for the quality of the designed resonant controller. Due to its characteristic of rejecting frequencies different from the ones it is tuned to, numerical errors from the discretization can change the expected behavior of the controller. Moreover, the presence of the intrinsic computational delay of digital systems with micro controllers can also alter this dynamic, and it is necessary to compensate for it as well.

Thus, the objective of this work is to present a novel discretization for the PR and VPI, named Real Zero Outside the Unic ircle (RZOUC), controllers that corrects the problems previously described. In addition, a novel algorithm is also proposed to optimize the closed loop stability of the discrete system, as well as to design the resonant compensators aiming to minimize the circulating harmonic currents.

A brief literature review on the discretizations of resonant controllers and their design methods is presented below. Section 2 presents and develops the proposed discretization for the PR and VPI controllers. Section 3 presents the proposed optimization by Inverse Nyquist Diagrams, while Section 4 presents the proposed design algorithm. Section 5 presents an application example for the proposed methodology, as well as the simulation results. Finally, Section 6 concludes the paper.

1.1 Resonant Controller Discretization Review

In Yepes et al. (2012), the author comprehensively reviewed and compared different forms of discretization for PR and VPI controllers. In addition, the effect of zeros on the discrete transfer functions of these controllers was also analyzed.

Later, the same group of authors proposed a correction to both resonance frequency and in the phase lead provided by the delay compensation (Yepes et al., 2010). This correction is achieved by correcting the poles and zeros placement.

Another work (Vidal et al., 2012) uses the technique described in (Yepes et al., 2012) to optimize the transient response of the discrete PR controller. In the same year, this technique is extended to the VPI controller (Vidal

⋆ We thank Petrobras for funding the R&D strategic project: ANEEL 00553-0046/2016 – "Technical and commercial arrangements for the insertion of energy storage systems in the Brazilian electricity sector", which allowed the idealization and accomplishment of this work.
This study was financed in part by the Coordenação de Aperfeiçoamento de Pessoal de Nível Superior - Brasil (CAPES) - Finance Code 001, and in part by the Conselho Nacional de Desenvolvimento Científico (CNPq).

et al., 2014), and a comparison between both controllers is performed.

A new discretization is proposed by Castro et al. (2016), where a modification to the optimal PR controller discretization analyzed by Yepes et al. (2010) and Yepes et al. (2012) is performed. While in the works of Yepes et. Al only one zero is allocated outside the unit circle, the discretization of Castro et. Al proposes that this zero is adjustable.

In (Pérez-Estévez et al., 2017), a novel discrete pole placement for LCL converters with resonant controller was proposed. With this proposal, no active damping is required to ensure stability.

The objective of this work is to expand the de Castro discretization for the VPI controller and further develop the mathematics behind this discretization.

1.2 Resonant Controller Design Review

In (Zmood et al., 1999), the PR controller is proposed, being capable of tracking sinusoidal signals with zero steady-state error. Its parameters design is a transformation of the PI parameters, and a comparison of both controllers is presented.

In (Lascu et al., 2007), the VPI resonant controller is proposed. The parameter design of this controller bases itself in the pole-zero cancellation technique.

Yepes et al. uses Nyquist diagrams to minimize the sensitivity function of the PR and VPI controller (Yepes et al., 2011). However, Nyquist diagrams of resonant controllers are not easy to analyze, since near the resonant frequency the gains go to infinity and the diagram diverges.

(Pereira et al., 2013) proposed a resonant controller design determined by means of a convex optimization problem with a set of linear-matrix-inequality constraints. The resultant controller, however, has 2 resonant gains, each one assigned to either sine or cosine dynamics.

(Kuperman, 2015) utilizes the same structure of (Pereira et al., 2013), aiming to the desirable transient performance. The controller gains are obtained directly through algebraic equations. However, it faces the same problem as that observed in (Pereira et al., 2013), that the resultant controller has two resonant gains.

(Pereira and Bazanella, 2015) proposes a PR controller design through the Ziegler-Nichols method. However, this method is not extended to VPI controllers.

A direct method for calculating PR controller gains was proposed in Pan-on and Sangtungtong (2019). This method cannot be extended to VPI controllers and has limitations regarding the overshoot of the closed loop system.

Thus, the objective of this work is to propose a design method based on the Inverse Nyquist Diagram of the open-loop system, where the smallest distance between this curve and the critical point $(-1, 0)$ would correspond numerically to the inverse of the Bode peak of the closed loop system.

2. THE PROPOSED RZOUC DISCRETIZATION

The continuous transfer functions for both the PR and VPI controllers is described in Eqs. (1) and (2), respectively.

$$H_{PR}(s) = K_p + K_r \frac{s}{s^2 + \omega_r^2} = K_p + K_r R_1(s) \quad (1)$$

$$H_{VPI}(s) = \frac{K_p s^2 + K_r s}{s^2 + \omega_r^2} = K_p R_2(s) + K_r R_1(s) \quad (2)$$

Where ω_r is the resonance frequency of the controllers, K_p and K_r are respectively the proportional and resonant controller gains, and $R_1(s)$ and $R_2(s)$ are the resonant dynamics for the PR and VPI controllers.

The realization of such controllers through digital microprocessors requires the development of difference equations that approximate the continuous system's characteristics. This is often done indirectly through processes referred to as discretization methods. Yepes et. al exhaustively compared different discretizations for resonant controllers, as this type of mathematical transformation directly affects the performance of the final controller. As a conclusion of the paper, the author suggested an optimum implementation that also compensates computational delay. Equations (3) and (4) exhibit the general discrete equations for the controllers, where

- $H_1(z)$ is a discrete time approximation for $R_1(s)$ using an impulse invariant transformation with computational delay compensation;
- $H_2(z)$ is a discrete time approximation for $R_2(s)$ using a Tustin with Prewarping transformation with computational delay compensation.

$$H_{PR}(z) = K_p + K_r H_1(z) \quad (3)$$

$$H_{VPI}(z) = K_p H_2(z) + K_r H_1(z) \quad (4)$$

The complete descriptions of $H_1(z)$ and $H_2(z)$ are given by equations (5) and (6), where h is the sampling period for the controllers and N is an integer corresponding to the number of sampling periods whose delays are to be compensated. According to the work of Yepes et. al, the optimal value for N is 1 or 2.

The complete equation for $H_2(z)$ can be rewritten as in equation (7), where $\alpha = 0.5 \sin(\omega_r h) \sin(\omega_r N h)$ and $\beta = \cos^2(0.5\omega_r h) \cos(\omega_r N h)$. The analyses for $H_2(z)$ are carried out with equation (7).

$$H_1(z) = hz \frac{z \cos(\omega_r h N) - \cos[\omega_r h (N-1)]}{z^2 - 2z \cos(\omega_r h) + 1}, \quad (5)$$

$$H_2(z) = \frac{\alpha(-z^2 + 1) + \beta(z^2 - 2z + 1)}{z^2 - 2z \cos(\omega_r h) + 1} \quad (7)$$

However, some drawbacks can be found when using the discretization approach described in (5), (7) and (6). In the case of systems in which ω_r is adaptive, and therefore variable, calculations are required at each iteration of each sine and cosine present in equations (5) and (7). This kind

of calculation may consume valuable interrupt period time in the microcontroller, which could be useful for other functions. Furthermore, the influence of the computational delay compensation N on the final controller is not made explicit, since different values of N will influence the zeros of the final controller.

Given these problems, the authors of this paper propose a new discretization method that enables both the PR and VPI controllers to compensate for the computational delay, as well as allocate the poles of the final controller in a way that improves the dynamics of the closed-loop system.

2.1 RZOUC-PR

$H_1(z)$ numerator has a root in zero and a second one that depends on ω_r, h and N. The second root can be found by solving equation (8):

$$z - \frac{\cos[\omega_r h(N-1)]}{\cos(\omega_r hN)} = 0. \tag{8}$$

Assuming that the product $\omega_r h$ is sufficiently small, both the cosines of the numerator and the denominator are in the first quadrant. This can be visualized in Figure 1. Since the argument of the denominator is greater than that of the numerator, the denominator will be a smaller real number than the also real numerator. Thus, dividing these cosines will result in a number greater than one. This means that this zero is real and outside the unit circle.

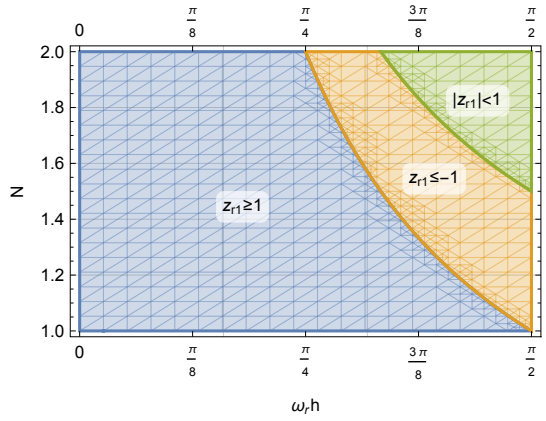

Figure 1. Regions showing zero behavior for the given parameters.

From this analysis, a possible discretization for a resonant compensator is that in (9).

$$H_1^{RZOUC}(z) = \frac{(hz)(z - z_{r1})}{z^2 - 2\cos(\omega_r h)\, z + 1} \tag{9}$$

The parameter z_{r1} is a real zero that can be allocated either inside or outside the unit circle. It also can influence the system's phase margin and can be adjusted to optimize stability margins. Thus, in the proposed discretization, the parameter to be optimized is z_{r1}, and not the computational delay compensation parameter N.

2.2 RZOUC-VPI

A similar procedure can be derived from (7), and its zeros can be rewritten as:

$$(z-1)\left(z - \frac{\beta+\alpha}{\beta-\alpha}\right) = 0 \tag{10}$$

The first zero of H_2 is fixed at 1. The second zero, which depends on the coefficients α and β, and consequently on the parameters ω_r, h and N, is not so simple to analyze analytically when compared to H_1. However, through the graph shown in Figure 2, it is also possible to reach the conclusion that the resulting zero will also be outside the unit circle.

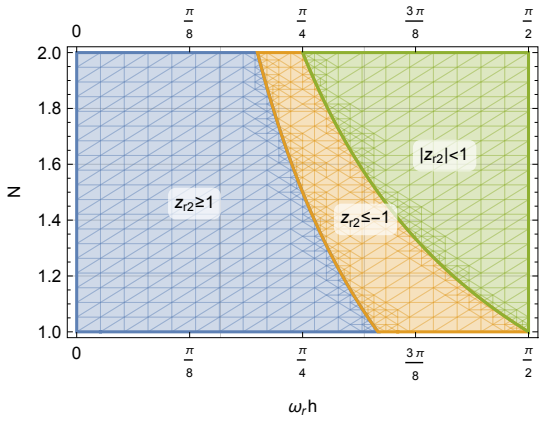

Figure 2. Regions showing zero behavior for the given parameters.

Similarly to (9), the proposed discretization for the VPI controller has also a real zero parameter z_{r2} that can be allocated inside or outside the unit circle. The proposed discretization is:

$$H_2^{RZOUC}(z) = \frac{(z-1)(z-z_{r2})}{z^2 - 2\cos(\omega_r h)\, z + 1} \tag{11}$$

3. OPTIMIZATION BY INVERSE NYQUIST DIAGRAMS

If one tries to take into account traditional stability margins when designing a controller based on resonant terms, specially considering harmonic frequencies, one might find multiple crossings of the 0 dB and $-180°$ lines in the open loop Bode diagram. One might then try inspecting the open loop Nyquist diagram, only to have to deal with the curve going to infinity at every resonant frequency. This nuisance can be dealt with as shown in Yepes et al. (2011).

The distance between the critical point for stability $(1, 0)$ in a Nyquist diagram and the curve given by the inverse of the open loop transfer function $H_{\text{open loop}}(z)$ is given by (12). The conclusion drawn in (12) is that said distance to the critical point $(1, 0)$ in the Nyquist diagram, for

$$H_2(z) = \frac{0.5(-z^2+1)\sin(\omega_r h)\sin(\omega_r Nh) + (z^2-2z+1)\cos^2(0.5\omega_r h)\cos(\omega_r Nh)}{z^2 - 2z\cos(\omega_r h) + 1} \tag{6}$$

a given frequency ω, of the open loop transfer function corresponds to the inverse of the closed loop Bode diagram magnitude at that frequency.

$$\begin{aligned}&\left|-1-\frac{1}{H_{\text{open loop}}\left(e^{j\omega h}\right)}\right| \\ &=\left|\frac{-\left(H_{\text{open loop}}\left(e^{j\omega h}\right)+1\right)}{H_{\text{open loop}}\left(e^{j\omega h}\right)}\right| \\ &=\left|\frac{1}{H_{\text{closed loop}}\left(e^{j\omega h}\right)}\right|\end{aligned} \tag{12}$$

A Nyquist diagram's smallest distance from the critical point $(1, 0)$ for the inverse, open loop transfer function can be interpreted as a stability margin M for that system. It can be expressed by the minimization of (12) as a function of ω, and alternatively as the maximization of its inverse, as given by equation (13).

$$M=\min_{\omega}\left|\frac{1}{H_{\text{closed loop}}\left(e^{j\omega h}\right)}\right|=\frac{1}{\max_{\omega}\left|H_{\text{closed loop}}\left(e^{j\omega h}\right)\right|} \tag{13}$$

Therefore, a stability margin is directly related to the peak magnitude of the closed loop Bode diagram.

If the open loop transfer function can be expressed as a function of a set of parameters $\bar{p}$, the stability margin can be written as $M(\bar{p})$ and taken as objective function in a maximization algorithm. The transfer function $H_{\text{closed loop}}(z)$ should then be redefined as $H_{\text{closed loop}}(z, \bar{p})$ Furthermore, let $H_{cl,peak}(\bar{p}) = \max_{\omega}\left|H_{\text{closed loop}}\left(e^{j\omega h}, \bar{p}\right)\right|$. Maximizing said stability margin then corresponds to minimizing the closed loop peak magnitude, as indicated by equation (14).

$$\begin{aligned}\max_{\bar{p}} M(\bar{p}) &= \max_{\bar{p}}\left\{\frac{1}{\max_{\omega}\left|H_{\text{closed loop}}\left(e^{j\omega h}, \bar{p}\right)\right|}\right\} \\ &= \frac{1}{\min_{\bar{p}}\left\{H_{cl,peak}(\bar{p})\right\}}\end{aligned} \tag{14}$$

The optimum parameter set for maximum stability margin is the one that gives the smallest closed loop peak, as indicated by equation (15).

$$\bar{p}_{opt} = \arg\max_{\bar{p}} M(\bar{p}) = \arg\min_{\bar{p}}\left\{H_{cl,peak}(\bar{p})\right\} \tag{15}$$

4. THE PROPOSED DESIGN ALGORITHM

Figure 3 exhibits the proposed design algorithm. The process starts by calculating the gains K_p and K_r for the PR and VPI fundamental frequency controllers. Here, methods based on pole-zero cancellation are used, however any preferred design method can be applied.

After calculating the gains of the fundamental controllers, a first stability optimization is performed on this system in order to obtain the first RZOUC values z_{r1} and z_{r2}. In this optimization, only z_{r1} and z_{r2} of the fundamental controllers are considered. The mathematical method described in Section IV is used here.

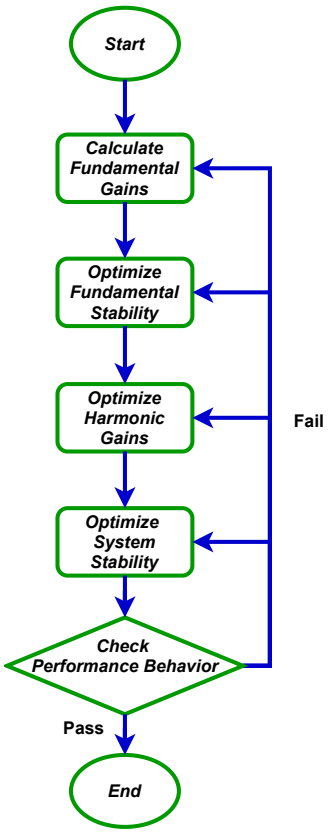

Figure 3. Flowchart of the proposed design algorithm

The next step in the proposed algorithm is to calculate the gains of harmonic compensators by optimizing the final harmonic current. The gains are calculated from the harmonic voltage of the bar where the converter connects.

A final stability optimization is applied, now considering the RZOUC of the fundamental, z_{r1} and z_{r2}, as much as those of the n harmonic compensators, z_{r1_n} and z_{r2_n}. For VPI harmonic compensators, the proportional gains K_{P_n} of the n-harmonics are also used to optimize stability, in conjunction z_{r1_n} and z_{r2_n}. Once the process is finished, it is verified if the resulting controller has the desired performance requirements. Each step of the algorithm will be explained in detail below. The mathematical model used here is in accordance with Castro et al. (2016) original work.

4.1 Fundamental Frequency Controllers Design

The 60 Hz fundamental frequency controllers' gains are calculated in the continuous domain. For this, two different design methods are used, one for the PR controller and one for the VPI controller: the Gao's method for the PR; and the pole-zero cancellation technique for the VPI.

Gao's method originally is a method applied to PI controllers, where pole cancellation with zero determines the closed-loop dynamics of the controller. However, through the transformation presented by Zmood and Holmes (2003), the gains of the PI controller can be transformed to the PR controller. Thus, the gains $K_{P_{Gao}}$ and $K_{R_{Gao}}$ are calculated as (16).

$$\begin{cases} K_{P_{Gao}} = \dfrac{T\omega_c}{K}; \\ \\ K_{R_{Gao}} = 2\dfrac{\omega_c}{K}. \end{cases} \tag{16}$$

In Gao's method, the PI controller design occurs through pole cancellation with zero, and after that the final PR controller is controlled. However, pole cancellation with zero between the plant and the PR controller does not occur in practice. In the VPI controller, the opposite occurs. The mathematical model of this controller allows the zero-pole cancellation to occur directly between the plant and the VPI. Thus, the gains $K_{P_{VPI}}$ and $K_{R_{VPI}}$ can be calculated according to (17).

$$\begin{cases} K_{P_{VPI}} = \dfrac{T\omega_c}{2K}; \\ \\ K_{R_{VPI}} = \dfrac{\omega_c}{2K}. \end{cases} \tag{17}$$

Both methods require the plant to have first-order behavior for their proper application. Equations (16) and (17) are based on a generic first-order system of the type:

$$H_{plant} = \frac{K}{Ts+1}. \tag{18}$$

Where K is the steady state gain, T is the time constant of the transfer function and ω_c is the desired system's bandwidth. As will be seen in Section 5, the LCL filter has a third-order transfer function, and it is not possible to use pole cancellation with zero directly. It was then considered that for the fundamental frequency the capacitive branch can be neglected, resulting in an equivalent first-order system with the inductors of the LCL filter in series connection.

4.2 Stability Optimization Procedure

Stability optimization aims to maximize stability by minimizing the closed loop peak, as shown in (14). The $\bar{p}$ parameters used for this optimization are the RZOUC z_{r1} and z_{r2} for the fundamental controller, and z_{r1_n} and z_{r2_n} the n-harmonic compensators. Thus, the optimization process takes place in two steps. The first of these, called partial optimization, optimizes only the RZOUC of the fundamental controllers. Once the gains of the harmonic compensators are calculated, the final stability final optimization optimizes the RZOUC and proportional harmonic gains of the compensators.

The vector of possible values of RZOUC is defined as $\bar{z_r} = (1, 9)$, i.e., the algorithm will search for real numbers equally spaced between limits 1 and 9 that maximize the closed-loop stability of the system. For the harmonic VPI controller, where the harmonic proportional gain K_{nP} is also used, a symmetric and equally spaced vector $\bar{K_P} = [-20K_{P_{VPI}}, 20K_{P_{VPI}}]$ is used.

This process is done numerically with the aid of MATLAB software, and one can use the preferred optimization method. Here brute force search is used, i.e., all possible combinations are tested, and then the one with the smallest closed loop peak in its frequency response is selected.

The desired stability criterion is that the disturbance rejection coming from the network is -40 dB between the frequencies of 59.9 and 60.1 Hz (Castro et al., 2016).

4.3 Harmonic Optimization Procedure

The resonant harmonic gains $K_{nR_{Gao}}$ and $K_{nR_{VPI}}$ are optimized so that the output current of the converter has the lowest possible harmonic composition. The vector of possible values $\bar{K_R} = [K_{nR_{min}}, K_{nR_{max}}]$ is constructed from the resonant gain of the fundamental current controller according to (19).

$$\begin{cases} K_{nR_{min}} = 10^{(\log_{10} K_R)-1} \\ K_{nR_{max}} = 10^{(\log_{10} K_R)+1} \end{cases} \tag{19}$$

The lower and upper bounds are calculated, respectively, one decade above and one decade below the fundamental resonant gain. In this way, the algorithm searches over a wider range of values. In addition, the vector of values is mirrored for negative magnitudes, such that $\bar{K}_{R_{final}} = [-\bar{K}_R, \bar{K}_R]$.

One then combines the possible values $\bar{K}_{R_{final}}$ with the desired harmonic compensators. For each of these combinations, the closed-loop disturbance transfer function $H_{dist}(z)$ – which can be considered the output admittance of the converter – is calculated. From this, the frequency response for the ω_n harmonic frequencies of interest are obtained. In possession of the harmonic grid voltage V_{th} and the frequency response of $H_{dist}(e^{j\omega_n h})$, the harmonic current is calculated by:

$$i_n = H_{dist}(e^{j\omega_n h}) v_{g_n}. \tag{20}$$

The currents i_n for each n-harmonic are then computed into the total harmonic current i_{total}. The goal of the optimization is to minimize the quadratic current i^2_{total}.

$$i^2_{total} = \sum i^2_n \tag{21}$$

For each $H_{dist}(z)$ generated from the different K_{nR} gain combinations of the harmonic compensators, there will be a i^2_{total} current associated with it. The combination of harmonic compensators that has the lowest i^2_{total} is then searched for.

5. APPLICATION EXAMPLE AND SIMULATION RESULTS

5.1 Application Example

The proposed controller design algorithm was applied in the PSCAD-EMTDC simulation environment to a 24 kVA inverter based on real equipment in the lab. Figure 4 shows the topology of the inverter and Table 1 shows its electrical parameters.

The variable to be fed back to the control is the converter current i_1. The block diagram of the complete control

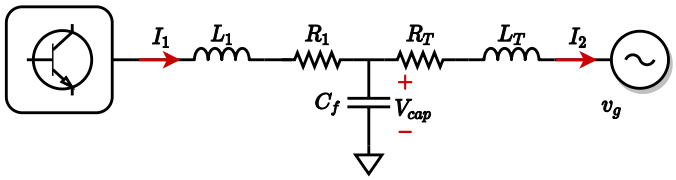

Figure 4. Converter topology.

Table 1. Parameters

Converter Parameters	
V_{LL} (V_{rms})	90
$S_{3\phi}$ (kVA)	24
V_{dc} (V)	300
Frequency (Hz)	60
Switching Frequency (Hz)	5100
Sampling Frequency (Hz)	10200
L_1 (μH)	600
R_1 (mΩ)	3.375
C_f (μF)	130
L_T (μH)	39,1
R_T (mΩ)	6.8

system is shown in Figure 5. Applying equations (16) and (17), with the desired $\omega_c = 250$ rad/s to this system, the resulting control gains are $K_{P_{Gao}} = 0.648$ and $K_{R_{Gao}} = 11.6$ for the PR controller, and $K_{P_{VPI}} = 0.324$ and $K_{R_{Gao}} = 2.9$ for the VPI controller.

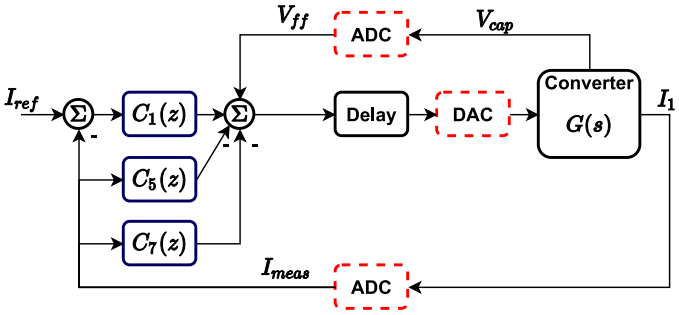

Figure 5. Controller block diagram.

After the fundamental controller gains are calculated, the partial stability optimization for this controllers is then performed. For the PR Controller, the fundamental RZOUC $z_{r1} = 1.32$, while for the VPI controller the fundamentals RZOUC are $z_{r1} = 1.0$ and $z_{r2} = 1.0$.

For the harmonic optimization, it is necessary to have the harmonic composition of the grid voltage to which the converter will be connected. Figure 6 shows the grid voltage waveform. It has 7% fifth harmonic and 5% seventh harmonic. From this input, the fifth and seventh harmonic compensation resonant gains can be calculated. For the PR controller, $K_{5R_{Gao}} = 24.6$ and $K_{7R_{Gao}} = 22.3$, while for the VPI controller $K_{5R_{VPI}} = 1.6$ and $K_{7R_{Gao}} = -76.6$.

The final stability optimization aims to calculate the harmonic gains of the RZOUC for both the PR and VPI controller, in addition to the harmonic proportional gains $K_{5P_{VPI}}$ and $K_{7P_{VPI}}$. For the PR controller, $z_{r1_5} = 2.28$ and $z_{r1_7} = 9.0$. For the VPI, $z_{r1_5} = 2.92$, $z_{r2_5} = 1.0$, $z_{r1_7} = 7.4$, $z_{r2_7} = 1.32$ as the RZOUC gains, $K_{5P_{VPI}} = 10.0$ and $K_{7P_{VPI}} = -2.0$ as the harmonic proportional gains. The

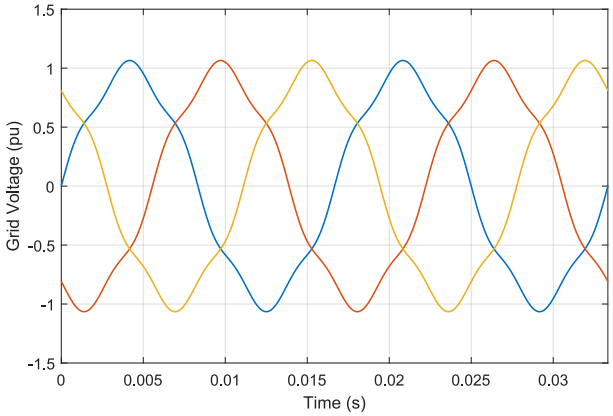

Figure 6. Grid voltage profile.

Bode diagrams for both the PR and VPI controllers is illustrated in Figure 7.

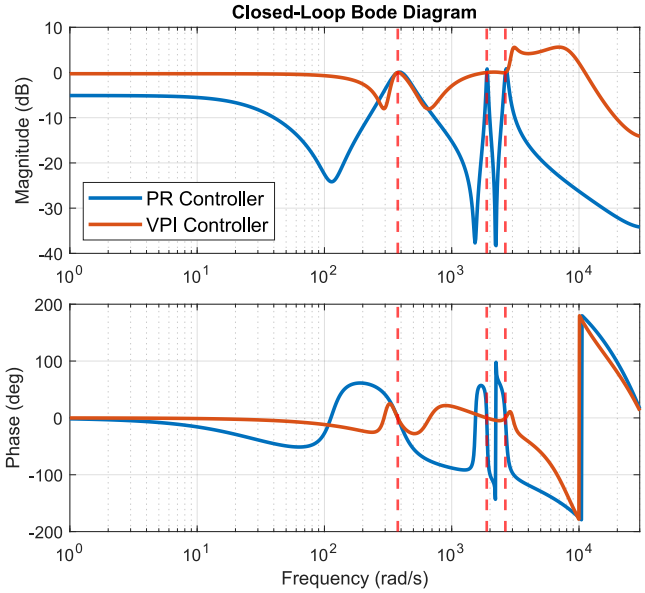

Figure 7. Tracking Bode diagrams for the PR, in blue, and VPI, in orange.

Figures 8 and 9 illustrates the smallest distance, which is associated with the peak from the frequency response, from the nyquist diagram for the critical point (-1,0) for the PR and VPI controllers respectively. The circle highlighted in green shows this distance tangent to the frequency where such a peak occurs, and that no other value violates this limit.

The PR controller has a peak of 0.789 dB at the frequency of 302.0125 Hz, the gain margin is 27.134 dB and the phase margin is 64.64 deg. The disturbance rejection is -39.8757 dB, being just above the established -40 dB criterion. Simulations with and without the presence of the harmonic compensators are depicted in Figures 10a and 10b, respectively.

The VPI controller has a peak of 5.6151 dB at the frequency of 1096.68 Hz, the gain margin is 5.103 dB and the phase margin is 32.2744 deg. The disturbance rejection is -41.46 dB, being just below the established -40 dB criterion. Simulations with and without the presence of

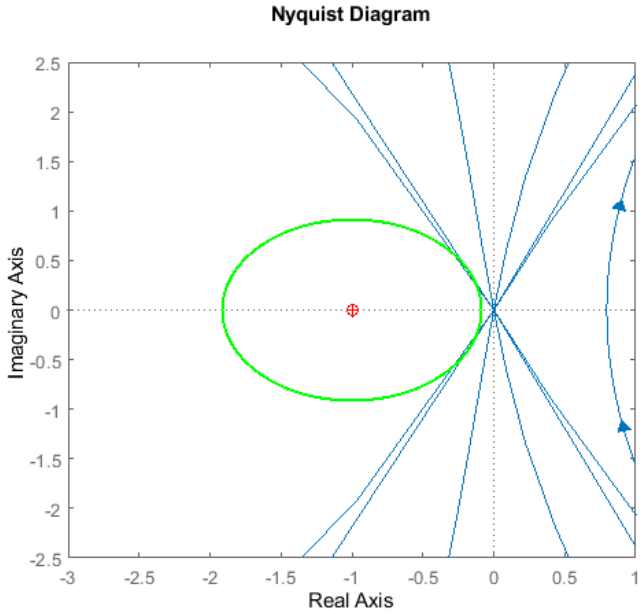

Figure 8. Critical distance between the (-1,0) point for the PR Inverse Nyquist Diagram.

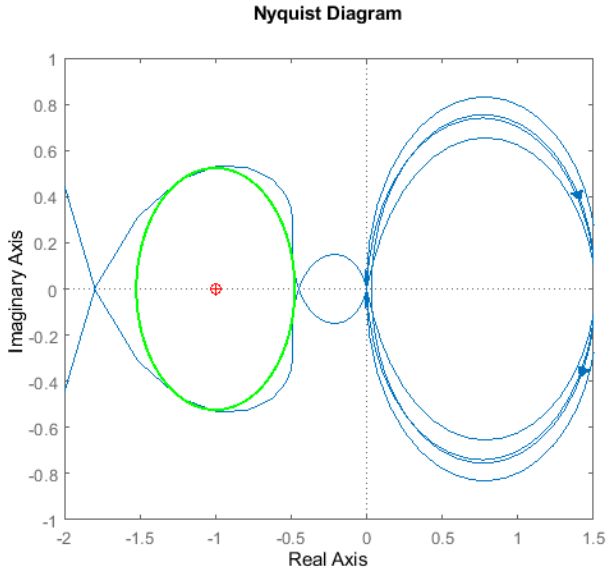

Figure 9. Critical distance between the (-1,0) point for the VPI Inverse Nyquist Diagram.

the harmonic compensators are depicted in Figures 12a and 12b, respectively.

5.2 Simulation Results

The simulation results are given below. The PR and VPI controllers with and without harmonic compensation will be compared transiently, as well as the current THD in the presence and absence of the compensations. At 0.05 s of simulation, the current sinusoidal references are changed from 0.0 p.u. to 1.0 p.u. of amplitude, thus meaning that the converter is injecting current and active power into the grid.

Figures 10a and 10b display the current reference step response for the PR controller without and with harmonic compensation, respectively. The presence of the harmonic compensators modify the transient response of the system, where there is a small increase in the settling time and oscillations of the system. However, the compensation of the harmonic currents is noticeable.

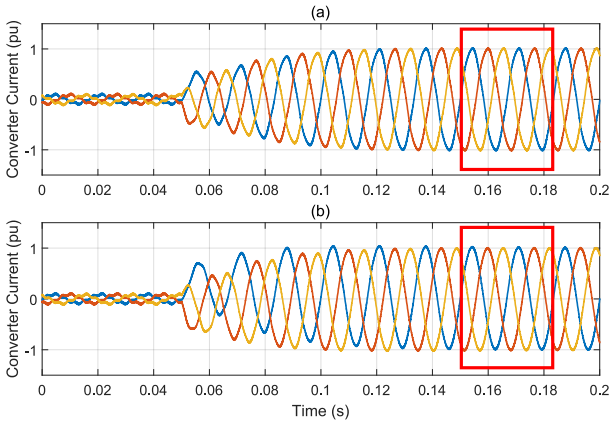

Figure 10. Comparison between current transitory behavior for the PR Controller without (a) and with (b) the harmonic compensators.

Figures 11a and 11b shows the current waveforms between the period of 0.15 s and 0.1833 s, corresponding to two 60 Hz cycles. This period corresponds to the area demarcated by the red rectangle in Figures 10a and 10b. Observing this time window, it is noticeable the complete elimination of the fifth and seventh harmonics in the converter current. The current THD has decreased from 11.85% to 0.55% after the addition of the harmonic compensators.

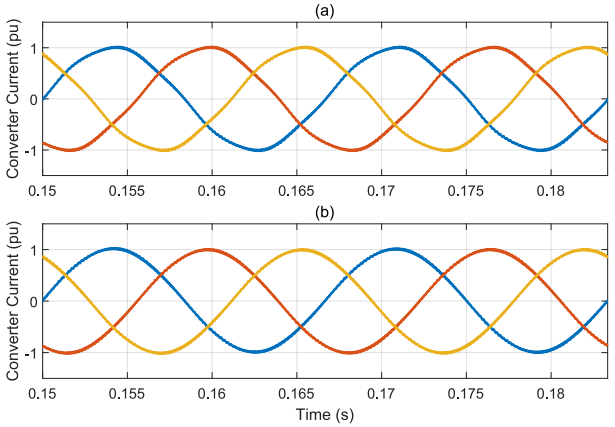

Figure 11. Comparison between current profiles for the PR Controller without (a) and with (b) the harmonic compensators.

The analyses performed for the PR controller can be done for the VPI controller. The current reference step response for this controller is shown in Figures 12a and 12b. Unlike the PR controller, the presence of the harmonic compensators did not change the transient dynamics of the VPI controller. Harmonic compensation is also noticeable in this scenario.

Figures 13a and 13b show in detail two current cycles in the presence and absence of the harmonic compensators, between 0.15 s and 0.1833 s . The current THD has decreased from 11.71% to 0.13% after the addition of the harmonic compensators.

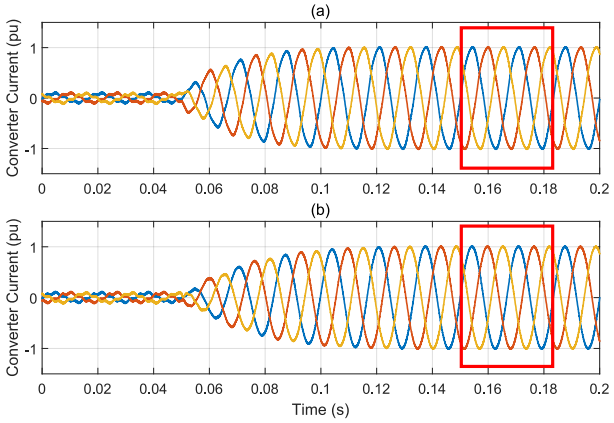

Figure 12. Comparison between current transitory behavior for the VPI Controller without (a) and with (b) the harmonic compensators.

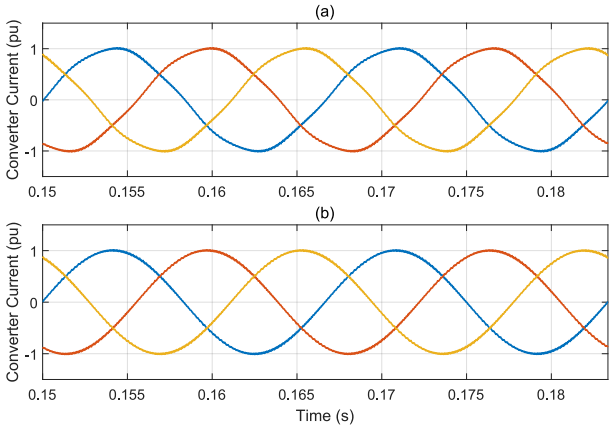

Figure 13. Comparison between current profiles for the VPI Controller without (a) and with (b) the harmonic compensators.

6. CONCLUSIONS

This paper presents a new discretization for the PR and VPI resonant controllers. From their mathematical model, the real zeros outside the unit circle serve as parameters to increase the stability margins of the system.

From the new discretization, the algorithm that optimizes the RZOUC parameters for increasing system stability from the concept of inverse Nyquist diagrams is also proposed. The algorithm also allows the optimized design of resonant harmonic compensators.

The design criteria were partially met , where only the VPI controller met the criteria and the PR controller being slightly off the established criteria. However, the simulation results show satisfactory dynamic behavior for both controllers, and validation of the harmonic compensators. Both the proposed discretization and the design algorithm have proven applicable and feasible for digital implementation of harmonic controllers.

REFERENCES

Castro, A.R., Gontijo, G.F., Guedes, S.D., Silva, L.F., Malateaux, E.C., Dias, R., and Aredes, M. (2016). Compensação de correntes harmônicas em STATCOM conectado a rede com tensão distorcida. In *Congresso Brasileiro de Automática*. Vitória. URL `http://www.swge.inf.br/proceedings/paper/?P=CBA2016-0676`.

Kuperman, A. (2015). Synchronous frame current controllers design based on desired stationary frame transient performance. *Electronics Letters*, 51(22), 1769–1770.

Lascu, C., Asiminoaei, L., Boldea, I., and Blaabjerg, F. (2007). High performance current controller for selective harmonic compensation in active power filters. *IEEE Transactions on Power electronics*, 22(5), 1826–1835.

Pan-on, J. and Sangtungtong, W. (2019). Design equation for directly computing two gains of pr controller. In *2019 IEEE 2nd International Conference on Power and Energy Applications (ICPEA)*, 119–123. IEEE.

Pereira, L.F.A. and Bazanella, A.S. (2015). Tuning rules for proportional resonant controllers. *IEEE Transactions on Control Systems Technology*, 23(5), 2010–2017.

Pereira, L.F.A., Flores, J.V., Bonan, G., Coutinho, D.F., and da Silva, J.M.G. (2013). Multiple resonant controllers for uninterruptible power supplies—a systematic robust control design approach. *IEEE Transactions on Industrial Electronics*, 61(3), 1528–1538.

Pérez-Estévez, D., Doval-Gandoy, J., Yepes, A.G., López, Ó., and Baneira, F. (2017). Enhanced resonant current controller for grid-connected converters with lcl filter. *IEEE Transactions on Power Electronics*, 33(5), 3765–3778.

Vidal, A., Freijedo, F.D., Yepes, A.G., Fernandez-Comesana, P., Malvar, J., López, Ó., and Doval-Gandoy, J. (2012). Assessment and optimization of the transient response of proportional-resonant current controllers for distributed power generation systems. *IEEE Transactions on Industrial Electronics*, 60(4), 1367–1383.

Vidal, A., Freijedo, F.D., Yepes, A.G., Malvar, J., López, Ó., and Doval-Gandoy, J. (2014). Transient response evaluation of stationary-frame resonant current controllers for grid-connected applications. *IET Power Electronics*, 7(7), 1714–1724.

Yepes, A.G., Freijedo, F.D., Doval-Gandoy, J., López, O., Malvar, J., and Fernández-Comesana, P. (2012). Correction to "effects of discretization methods on the performance of resonant controllers". *IEEE Transactions on Power Electronics*, 27(12).

Yepes, A.G., Freijedo, F.D., López, O., and Doval-Gandoy, J. (2010). High-performance digital resonant controllers implemented with two integrators. *IEEE Transactions on Power Electronics*, 26(2), 563–576.

Yepes, A.G., Freijedo, F.D., Lopez, O., and Doval-Gandoy, J. (2011). Analysis and design of resonant current controllers for voltage-source converters by means of nyquist diagrams and sensitivity function. *IEEE transactions on industrial electronics*, 58(11), 5231–5250.

Zmood, D.N. and Holmes, D.G. (2003). Stationary frame current regulation of pwm inverters with zero steady-state error. *IEEE Transactions on power electronics*, 18(3), 814–822.

Zmood, D.N., Holmes, D.G., and Bode, G. (1999). Frequency domain analysis of three phase linear current regulators. In *Conference Record of the 1999 IEEE Industry Applications Conference. Thirty-Forth IAS Annual Meeting (Cat. No. 99CH36370)*, volume 2, 818–825. IEEE.